Supporting information

Dysfunctional Conformational Dynamics of Protein Kinase A Induced by a Lethal Mutant of Phospholamban Hinder Phosphorylation

*Jonggul Kim[1], Larry R. Masterson[2], Alessandro Cembran[1,2], Raffaello Verardi[2], Lei Shi[1], Jiali Gao[1], Susan S. Taylor[4] and Gianluigi Veglia[1,2]**

[1]Department of Chemistry– University of Minnesota, Minneapolis, MN 55455.

[2]Department of Biochemistry, Molecular Biology, and Biophysics- University of Minnesota, Minneapolis, MN 55455;

[3]Present address: Department of Chemistry and Biochemistry, University of Minnesota Duluth, Duluth, MN 55812

[4]Howard Hughes Medical Institute, Department of Chemistry and Biochemistry, University of California at San Diego, CA 92093

* To whom correspondence should be addressed:

Gianluigi Veglia, Department of Biochemistry, Biophysics, and Molecular Biology, University of Minnesota, 6-155 Jackson Hall, MN 55455. Telephone: (612) 625-0758. Fax: (612) 625-2163. E-mail: vegli001@umn.edu.

Susan Taylor, Department of Chemistry and Biochemistry, University of California San Diego, 9500 Gilman Dr. CMM W125 La Jolla, CA 92093, Ph: (858) 534-8190, Fax: (858) 534-8193

E-mail : staylor@ucsd.edu

SI Materials and Methods

Lactic dehydrogenase (LDH) and pyruvate kinase (PK) were purchased from Sigma (Solon, Ohio, USA). Adenosine 5'-triphosphate (ATP), phosphoenolpyruvate (PEP), magnesium chloride, and reduced nicotinamide adenine dinucleotide (NADH) were purchased from Sigma Aldrich (St. Louis, MO, USA).

Sample Preparation. Final concentrations for ITC measurements were between ~30 μM of PKA-C as confirmed by A_{280} = 52060 M^{-1} cm^{-1}. 2 mM of ATPγN was used for a nucleotide saturated state. All ITC measurements were performed with a Microcal VP-ITC instrument at 27°C. Approximately 1.7 mL of PKA-C was used for each experiment and 280 μL of 1.0-1.2mM of PLN_{1-19} or $R14del_{1-19}$ in the titrant syringe. All experiments were performed in duplicate or triplicate. The heat of dilution of the ligand to the buffer was measured and subtracted from the experiment accordingly. Binding was assumed to be 1:1 and was analyzed using the Wiseman Isotherm[1] using the NanoAnalyze software.

$$\frac{d[MX]}{d[X_{tot}]} = \Delta H \cdot V_0 \left[\frac{1}{2} + \frac{1-(1+r)/2-R_m/2}{(R_m^2 - 2R_m(1-r)+(1+r)^2)^{1/2}} \right] \quad (1)$$

where the change of the total complex, d[MX] with respect to the change of the ligand concentration, $d[X_{tot}]$ is dependent on r, the ratio of the K_d with respect to the total protein concentration, and R_m, the ratio between the total ligand and total protein concentration. The free energy of binding was determined using the following:

$$\Delta G = RT \ln K_d$$

Where R is the universal gas constant and T is the temperature at measurement (300K). The entropic contribution to binding was calculated using the following:

$$T\Delta S = \Delta H - T\Delta S$$

NMR spectroscopy. Samples for triple resonance assignment experiments were made to a concentration ~0.4-0.8 mM in 20 mM KH_2PO_4, 90 mM KCl, 10 mM DTT, 10 mM $MgCl_2$ 1 mM NaN_3 at pH 6.5. 12 mM ATPγN was added for the binary complex and 12 mM ATPγN with 1.0 mM of PKI_{5-24} and 60 mM $MgCl_2$ was added for the closed form complex. All experiments were performed on a 850 MHz Bruker Advance III spectrometer equipped with a TCI cyroprobe. All experiments were performed at 300K. All data was processed using NMRpipe[2], and visualized using Sparky.

The TROSY-based[3, 4] HNCA and HN(CO)CA experiments were collected with a minimum of 24 scans, 2048 (proton), 64 (nitrogen), and 80 (carbon) complex points and the TROSY-based HN(CA)CB and HN(CO)CACB experiments were collected with a minimum of 32 scans, 2048 (proton), 64 (nitrogen) and 100 (carbon) complex points were performed to measure the $^{13}C^{\alpha}$ and $^{13}C^{\beta}$ correlations. All ^{1}H-^{15}N Trosy-HSQC experiments were acquired with 2048(proton) and a minimum of 100(nitrogen) complex points. Combined chemical shift perturbations were calculated using amide 1H and 15N chemical shifts according the following:

$$\Delta\delta = \sqrt{\Delta\delta_H^2 + 0.154\Delta\delta_N^2} \qquad (2)$$

$^{15}N[^{1}H]$-NOE values[5] were determined by the ratio of signal intensity from TROSY-select[6] experiments with and without ^{1}H saturation of 5 s. Error was calculated from error propagation of the root mean square noise. Mapping of slow conformational dynamics was performed by utilizing the Trosy Hahn-Echo method[7]. This modified transverse relaxation optimized experiment allows for the measurement of α, β and longitudinal two spin order (zz) during a Hahn echo period set to $2/J_{NH}$ (10.8 ms). The R_{ex} value was computed as the following[8]:

$$R_{ex} \approx C_{zz} \ln \rho_{zz} + C_{\beta} ln\rho_{\beta} \qquad (3)$$

where $C_{zz} = (2\tau)^{-1}$, $C_{\beta} = (<\kappa>-1)(4\tau)^{-1}$, $\kappa = 1- 2*\ln\rho_{zz}/\ln\rho_{\beta}$, $\rho_{zz} = I_{zz}/I_{\alpha}$, and $\rho_{\beta} = I_{\beta}/I_{\alpha}$. <κ> was determined from the trimmed mean from the resonances that did not exhibit chemical exchange. All data was acquired in an interleaved fashion and standard deviation was calculated from error

propagation from the root mean square noise of the data. Residues with R_{ex} were qualitatively identified by measuring the change in the inverse peak height with increasing temperature as described previously[8].

Analysis of the Chemical Shift Perturbations

We employed the COordiNate ChemIcal Shift bEhavior (CONCISE)[9] method to monitor trajectories of chemical shifts and measure the change in equilibrium position associated with each PKA-C construct (apo, ATPγN, ATPγN/PLN^{R14del}, ATPγN/PLN^{WT}, and ATPγN/PKI). In short, through Principal Component Analysis (PCA), the method identifies a set of residues whose chemical shifts respond linearly to the conformational transition. Each one of these residues provides a measure of the equilibrium position for every PKA-C construct in form of scores along the first principal component. The equilibrium position for a given construct is given by the average of the PC-scores over all linear residues.

To identify the residues whose chemical shifts follow a linear pattern, a threshold of 3.0 for the ratio of the standard deviations of PC1 over PC2 was used, and residues that were affected by chemical shifts perturbations below 0.05 ppm were also discarded (see [9]for details on the threshold calibration). After these thresholds were applied, a total of 105 residues formed the subset that was used to trace the equilibrium position of each state (see Table S4). To identify the largest group of residues that respond to ligand binding in a correlated fashion, an adapted[9] version of the chemical shift covariance analysis[10] (CHESCA) was applied to the PCA projection of the chemical shifts. First, the correlation matrix between all linear residues' PC1 projections was constructed (**Figure S5B**) and used to build a dendrogram through hierarchical clustering. The dendrogram was then cut at a 0.97 level of correlation coefficient, which has been shown to be appropriate to identify correlated clusters of residues[10]. We notice that only a handful of residues were filtered out by the CHESCA analysis from the linear subset identified through CONCISE (residues 76, 176, 226, 306, and 336), which confirms that

those residues' chemical shifts not only respond *linearly* to ligand binding, but they all also respond in a *correlated* way.

Dynamic Light Scattering

Samples prepared for NMR relaxation experiments were evaluated with a Malvern Zetasizer μV system. 100 μL of sample was placed in a polystyrene micro cuvette and equilibrated for five minutes at 298K Measurements were made after automatic optical adjustment and six runs were collected, each run consisting of an average of eleven measurements. The Z-average diameter, reporting on the hydrodynamic radius of the protein, was from a cumulate analysis of the measured intensity autocorrelation function using the Zetasizer software Version 6.34. Assuming isotropic molecular tumbling, the rotation correlation time (τ_c) was calculated using the Stokes-Einstein equation at 300K.

MD simulations

The ternary complex PKA-C/ATPγN/PLN was obtained from molecular docking calculations as described previously[11]. The system was solvated in a cubic box of 80 x 80 x 80 $Å^3$ using a TIP3P water model. Counter ions were added to reach neutrality and an ionic strength of ~150 mM. All of the simulations were set up using CHARMM c36a1 [12] and performed with NAMD 2.7b1[13]. CHARMM27 force field [14] with CMAP correction [15] was used for all of the calculations. After initial minimization, the system was gradually heated from 10 to 310 *K* every 30 *K* using 10 ps of NPT simulations at each temperature. During energy minimization and heating, harmonic restraints were kept on non-water and non-counter ions and gradually decreased from 25 to 3 $kcal/mol*Å^2$. Harmonic restraints with a force constant (3 $kcal/mol*Å^2$) were applied to all protein heavy atoms during the initial 5 *ns*. The simulations were carried out at 310 *K* employing Langevin dynamics with a damping constant of 1.0 ps^{-1} and at 1 *atm* using a Nosé-Hoover Langevin piston pressure control[16]**.** Long-range electrostatic interactions were calculated using a particle-mesh Ewald (PME) summation[17]. Non-bonding interactions were calculated using a cutoff radius of 9 Å. Rattle algorithms were applied to all bonds involving

hydrogen atoms[18]. The equations of motion were integrated using r-RESPA multiple time step scheme[19] with a time step of 2 fs. The system was simulated for a total of 80 *ns*.

The last 25 ns of both WT and R14Del MD trajectories (saved every 1 ps) were used to calculate the root mean square fluctuation (RMSF) for each residue of the kinase. First, as in reference[11], the trajectories were aligned by overlaying the backbone atoms (N, Cα, and C) of the E and F helices (residues 140-160 and 217-233). Next, the backbone RMSF for the n^{th} residue *RMSF(n)* was calculated as a per-residue average over the N, Cα, and C atoms:

$$RMSF(n) = \frac{1}{3} \sum_{i=N,C\alpha,C} \sqrt{\frac{1}{3N} \sum_{j=1}^{N} \sum_{q=x,y,z} (q_i^n(j) - \langle q_i^n \rangle)^2}$$

Where the index *j* runs over all the time frames N, and $\langle q_i^n \rangle$ is the average coordinate of the atom *i* of residue *n*.

The results were plotted in **Figure S12D** for the WT and R14Del trajectories individually, and as the difference between the R14Del and WT RMSF in **Figure S12E**.

Figure Captions

Figure S1. A) ITC thermographs of titrations of PLN_{1-19}^{WT} to Apo PKA-C (black), PLN_{1-19}^{WT} to ATPγN saturated PKA-C (green) and PLN_{1-19}^{R14del} to ATPγN saturated PKA-C (orange). **B**) Substrate concentrations of 10-300 μM and PKA-C concentration of 64 nM and **C**) substrate concentrations of 100-900 μM and PKA concentration of 256 nM.

Figure S2. ^{1}H-^{15}N TROSY-HSQC spectra for PKA-C/ATPγN (violet), PKA/C PLN_{1-19}^{R14del} (orange), PKA-C/ PLN_{1-19}^{WT} (green) and PKA-C/PKI_{5-24} form (red).

Figure S3. The random coil chemical shift index for the backbone carbon atoms for the Apo PKA-C, PKA-C/ATPγN (binary) and PKA-C/PKI_{5-24} (closed) form. 92%, 89% and 94% of the observable resonances for apo, binary and closed were assigned. Note since that ATPγN form experiences significant conformational exchange, the least number of resonances are observed.

Figure S4. Strip plots of resonance assignment experiments for a section of the glycine-rich loop (I46 to G50) corresponding to the **A**) $^{13}C\alpha$ and **B**) $^{13}C\beta$ chemical shifts from Trosy-based HNCA/HN(CO)CA/HN(CA)CB/HN(CO)CACB experiments.

Figure S5. A) Scatter plot of the chemical shift perturbation with binding of PLN_{1-19}^{WT} and PLN_{1-19}^{R14del} to PKA-C/ATPγN **B**) CHESCA analysis[10] of the chemical shifts shows the largest cluster of coordinated chemical shifts to be dispersed throughout the enzyme.

Figure S6: Residues that are broadened beyond detection with PLN_{1-19}^{R14del} but are present with PLN_{1-19}^{WT} (red) and were too weak to be detected using NMR relaxation studies (orange) Note that many of the missing residues are along catalytically important regions

Figure S7: CONCISE analysis of the backbone chemical shifts including PKA-C/ATPγN/Kemptide as a second Michealis complex.

Figure S8. The dynamic light scattering data for PKA-C/PLN_{1-19}^{WT} and PKA-C/$\mathrm{PLN}_{1-19}^{R14del}$ and PKA-C/ATPγN. The raw scattering correlation plot for all runs as well as the size of the particles from the fit are shown.

Figure S9. A) NMR analysis of picosecond to nanosecond dynamics of ternary complex of PKA-C/PLN_{1-19}^{WT} and PKA-C/$\mathrm{PLN}_{1-19}^{R14del}$. **B)** NMR analysis of microsecond to millisecond dynamics of the same complexes were performed using the Trosy Hahn-Echo experiments. The negative NOE values and the apparent R_{ex} values along the first 15 residues on the N-terminus result from these residues being disordered with respect to the rest of the protein, resulting in a very small apparent τ_c. **C)** Change of the inverse peak height with respect to temperature for PKA-C/PLN_{1-19}^{WT} and PKA-C/$\mathrm{PLN}_{1-19}^{R14del}$.

Figure S10. Backbone dynamics of the ternary complexes of PLN_{1-19}^{WT} and $\mathrm{PLN}_{1-19}^{R14del}$. **A)** Mapping of HX NOE for the ternary complex of PLN_{1-19}^{WT} and $\mathrm{PLN}_{1-19}^{R14del}$ **B)** Mapping of Rex from Trosy Hahn-Echo for the ternary complex of PLN_{1-19}^{WT} and $\mathrm{PLN}_{1-19}^{R14del}$.

Figure S11. A) Mapping of R_{ex} around the N-terminus of PKA-C on the PKA-C/ATPγN, PKA-C/PLN_{1-19}^{WT} and PKA-C/$\mathrm{PLN}_{1-19}^{R14del}$ bound forms. Conformational exchange is propagated from the C-helix to the αC-β1 linker. **B**) R_{ex} of PKA-C/ ATPγN along the C-terminus and the F-helix.

Figure S12. A) Time-dependent distances between guanidino groups of Arg side chains and the nearest neighbors within the active site in PKA-C/PLN_{1-19}^{WT}. **B**) Time course of the torsion angles during the MD simulations. **C**) Time course of the Arginine-phosphate distance during the MD simulations. **D**) RMSF analysis of the trajectories of PKA-C/PLN_{1-19}^{WT}[11] and PKA-C/$\mathrm{PLN}_{1-19}^{R14del}$ **E**) Difference of the RMSF between PKA-C/$\mathrm{PLN}_{1-19}^{R14del}$ and PKA-C/PLN_{1-19}^{WT}.

Figure S1.

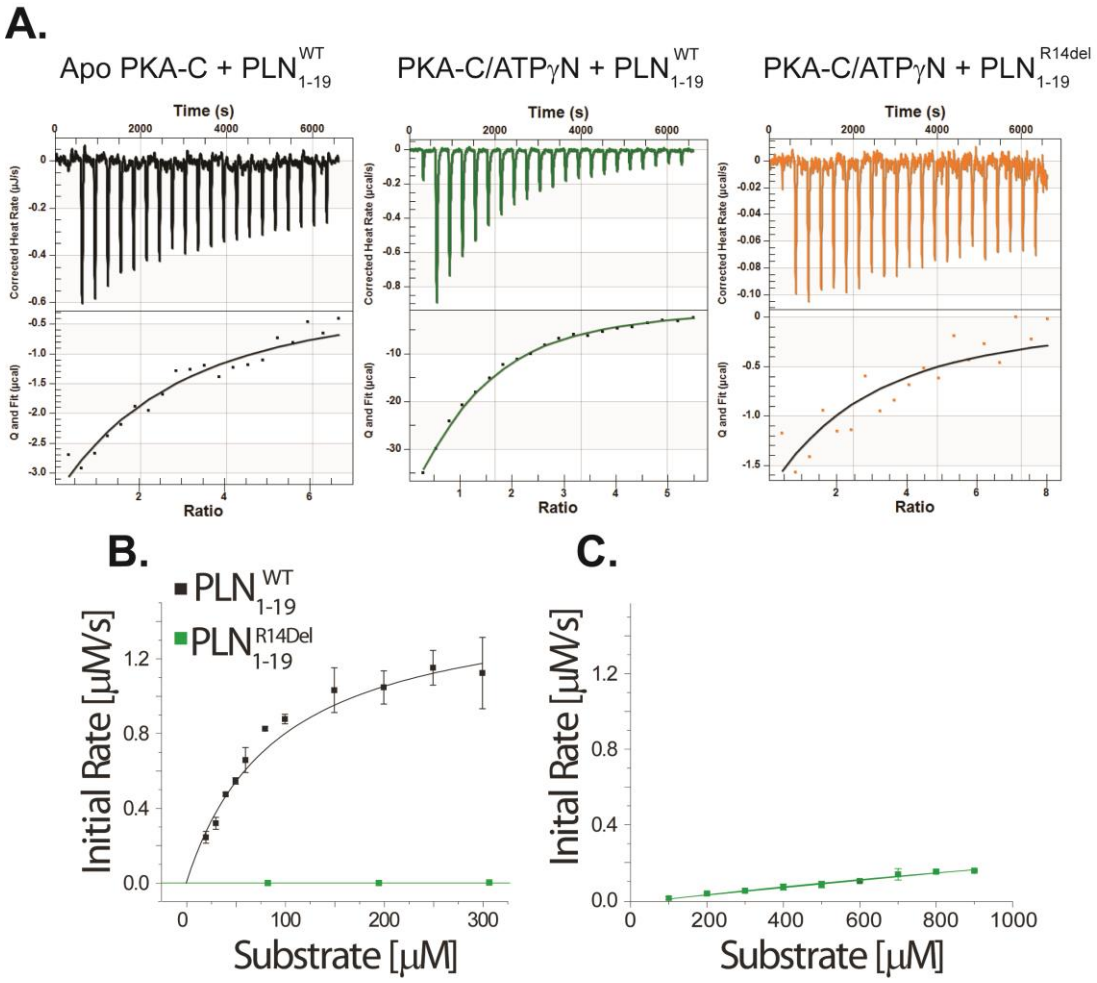
A.
Apo PKA-C + PLN 1-19 WT
PKA-C/ATPγN + PLN 1-19 WT
PKA-C/ATPγN + PLN 1-19 R14del
Time (s)
Corrected Heat Rate (µJ/s)
Corrected Heat Rate (µcal/s)
Q and Fit (µcal)
Ratio
B.
PLN 1-19 WT
PLN 1-19 R14Del
Initial Rate [µM/s]
Substrate [µM]
C.
Inital Rate [µM/s]
Substrate [µM]

Figure S2

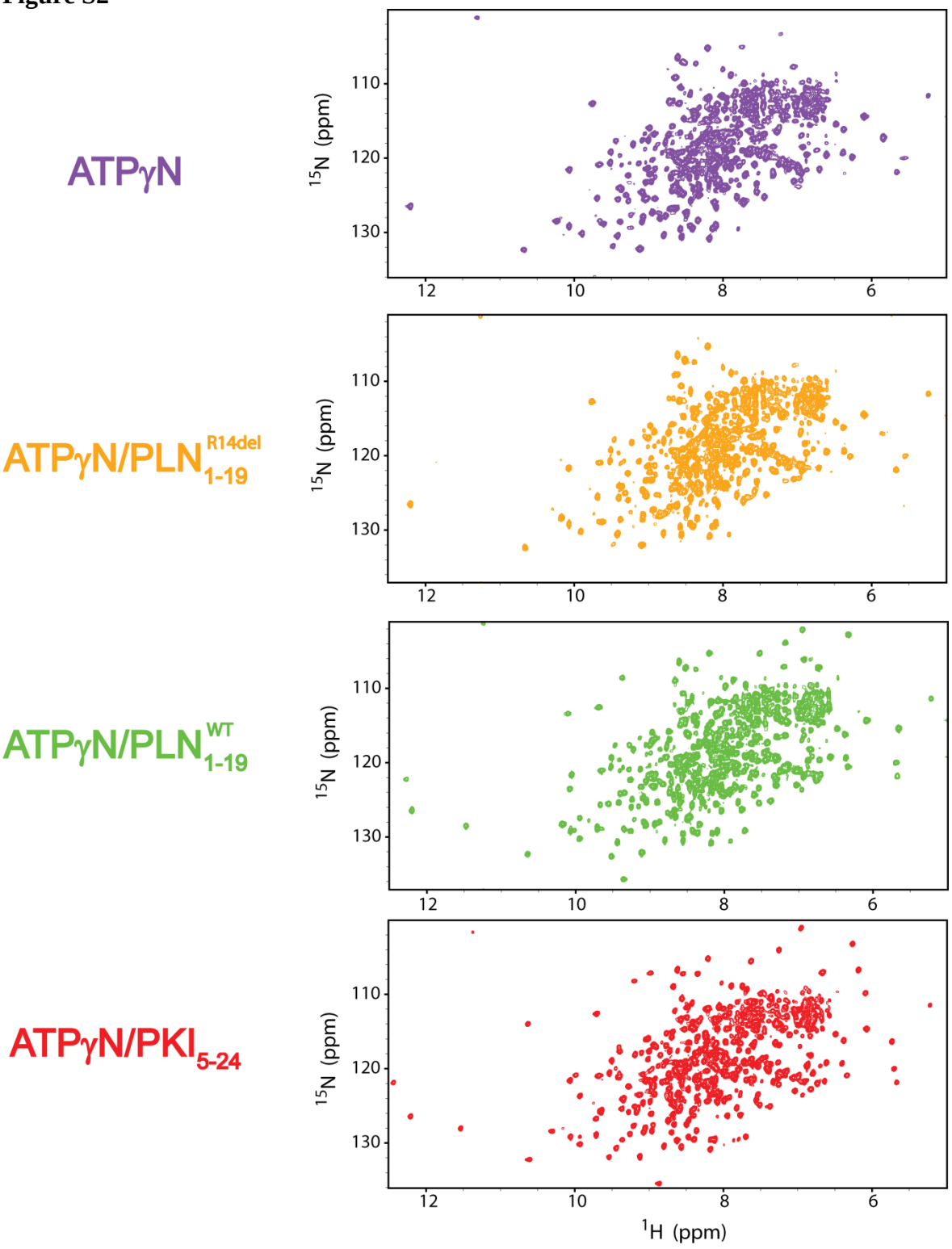
ATPγN
ATPγN/PLN R14del 1-19
ATPγN/PLN WT 1-19
ATPγN/PKI 5-24
15N (ppm)
110
120
130
12
10
8
6
1H (ppm)

Figure S3

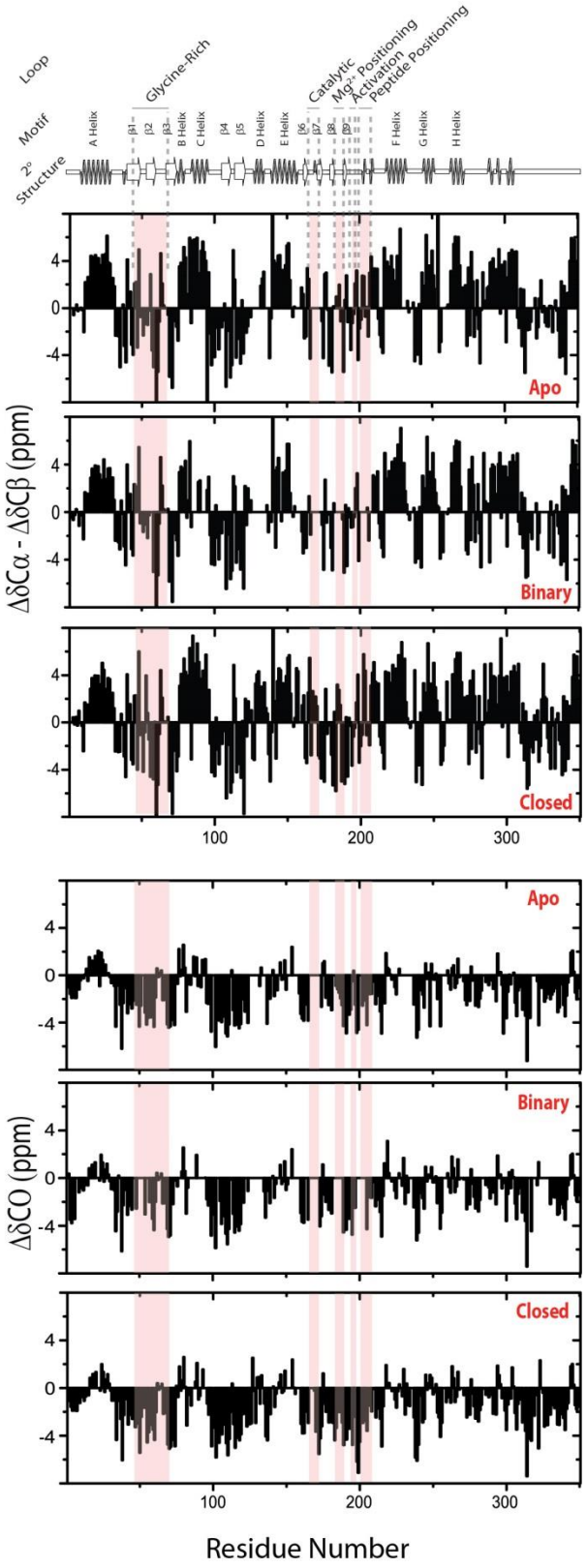
Loop
Motif
2° Structure
Glycine-Rich
Catalytic
Mg2+ Positioning
Activation
Peptide Positioning
A Helix
β1
β2
β3
B Helix
C Helix
β4
β5
D Helix
E Helix
β6
β7
β8
β9
F Helix
G Helix
H Helix
ΔδCα - ΔδCβ (ppm)
Apo
Binary
Closed
ΔδCO (ppm)
Apo
Binary
Closed
4
0
-4
100
200
300
Residue Number

Figure S4

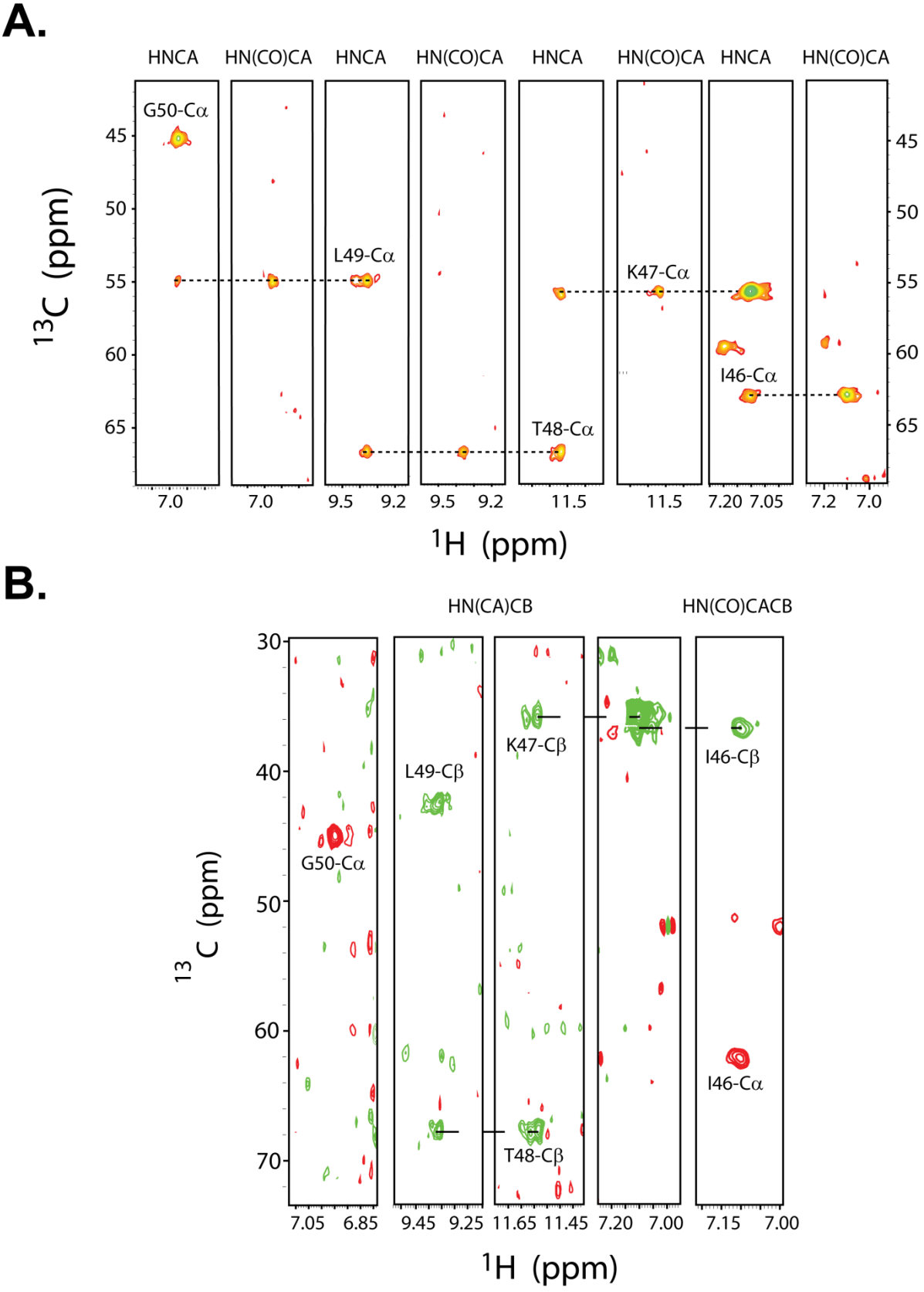
A.
HNCA
HN(CO)CA
HNCA
HN(CO)CA
HNCA
HN(CO)CA
HNCA
HN(CO)CA
G50-Cα
L49-Cα
K47-Cα
I46-Cα
T48-Cα
13C (ppm)
1H (ppm)
B.
HN(CA)CB
HN(CO)CACB
G50-Cα
L49-Cβ
K47-Cβ
I46-Cβ
T48-Cβ
I46-Cα
13C (ppm)
1H (ppm)

Figure S5

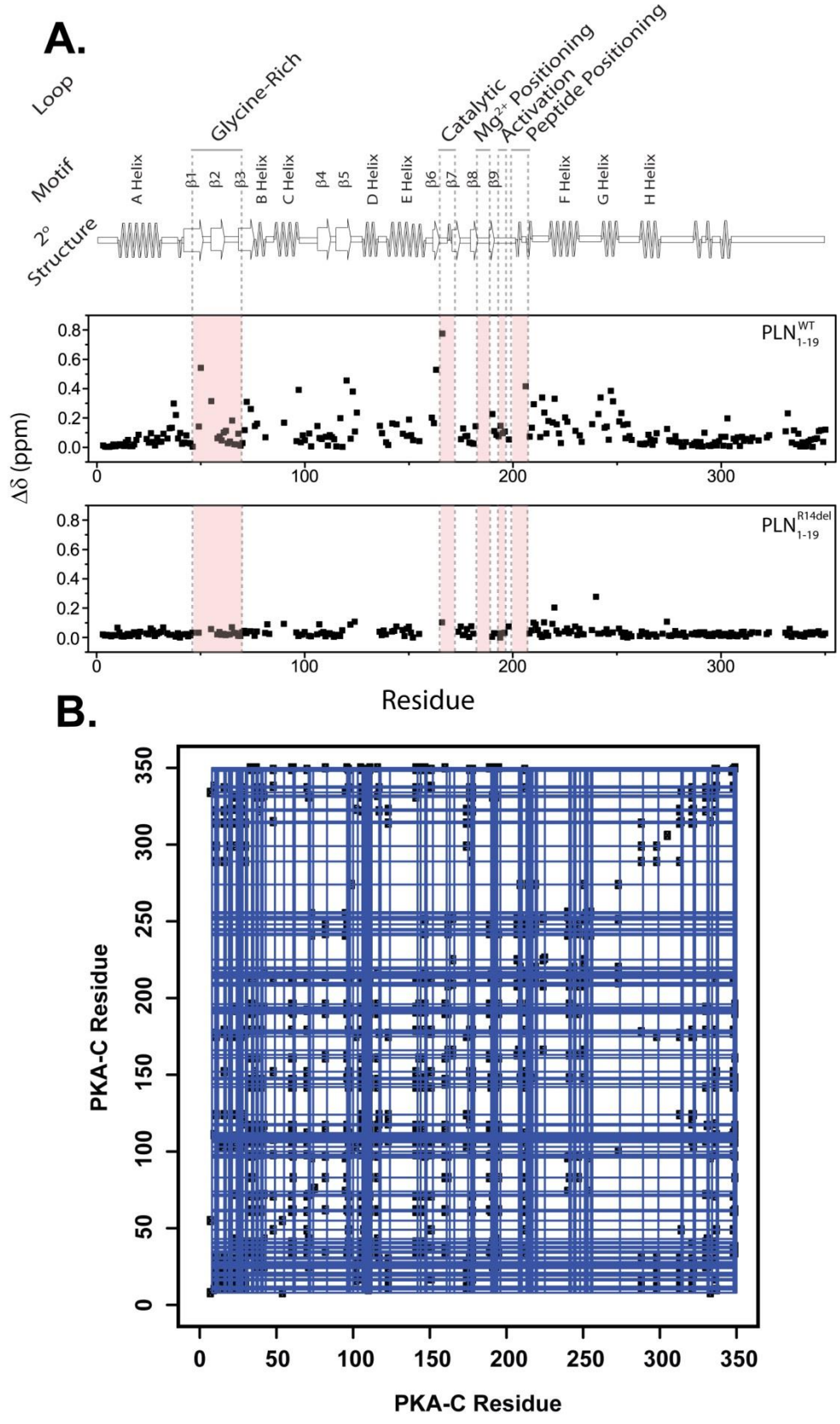
A.
Loop
Motif
2° Structure
Glycine-Rich
Catalytic
Mg2+ Positioning
Activation
Peptide Positioning
A Helix
β1
β2
β3
B Helix
C Helix
β4
β5
D Helix
E Helix
β6
β7
β8
β9
F Helix
G Helix
H Helix
PLN1-19WT
PLN1-19R14del
Δδ (ppm)
Residue
B.
PKA-C Residue
PKA-C Residue

Figure S6

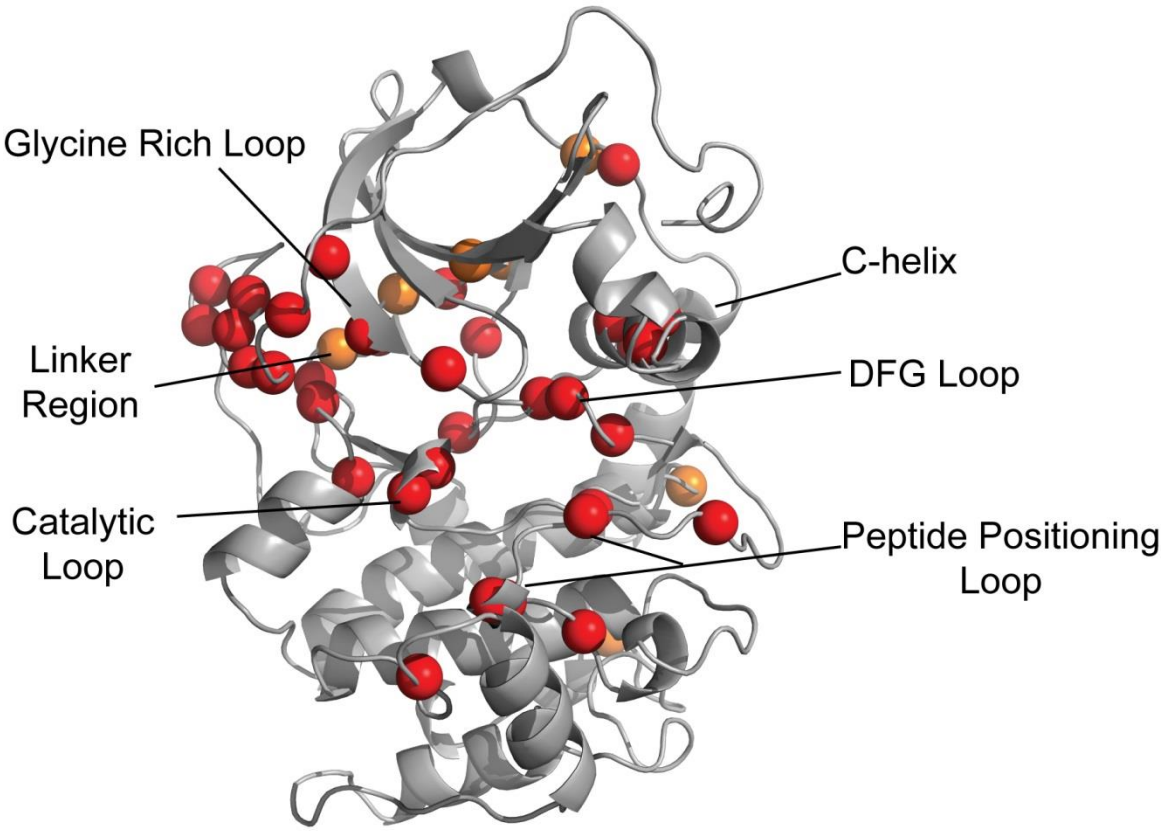
Glycine Rich Loop
C-helix
Linker Region
DFG Loop
Catalytic Loop
Peptide Positioning Loop

Figure S7

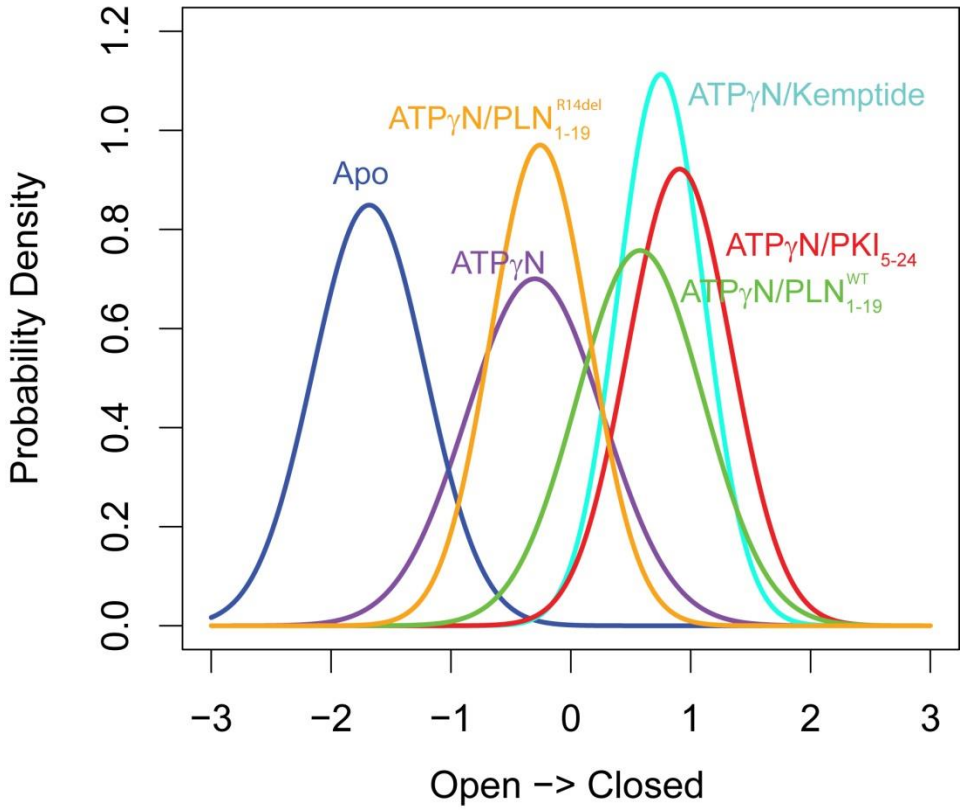
Probability Density
0.0
0.2
0.4
0.6
0.8
1.0
1.2
−3
−2
−1
0
1
2
3
Open −> Closed
Apo
ATPγN/PLN R14del 1-19
ATPγN
ATPγN/Kemptide
ATPγN/PKI 5-24
ATPγN/PLN WT 1-19

Figure S8

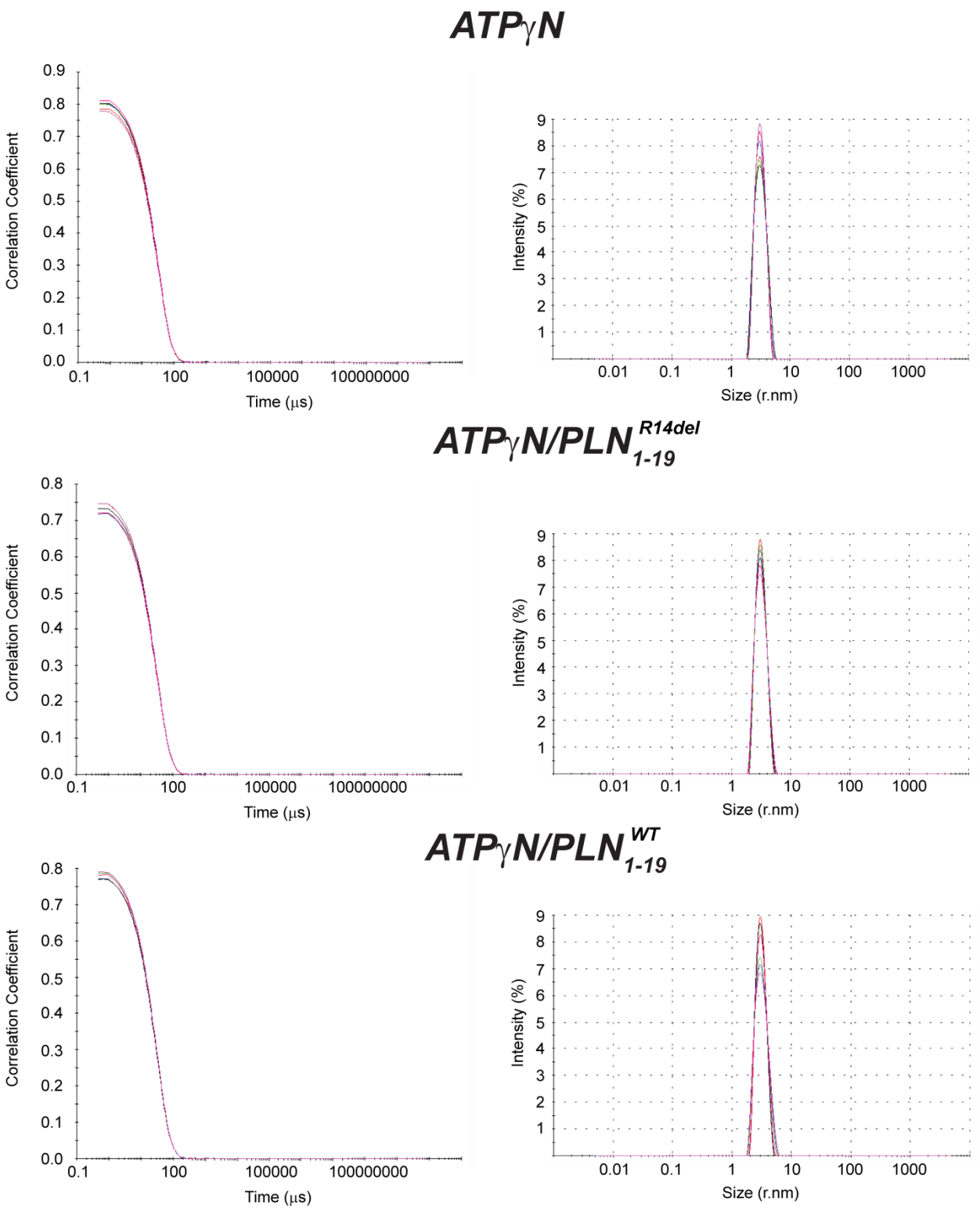
ATPγN
Correlation Coefficient
Time (μs)
Intensity (%)
Size (r.nm)
ATPγN/PLN R14del 1-19
Correlation Coefficient
Time (μs)
Intensity (%)
Size (r.nm)
ATPγN/PLN WT 1-19
Correlation Coefficient
Time (μs)
Intensity (%)
Size (r.nm)

Figure S9

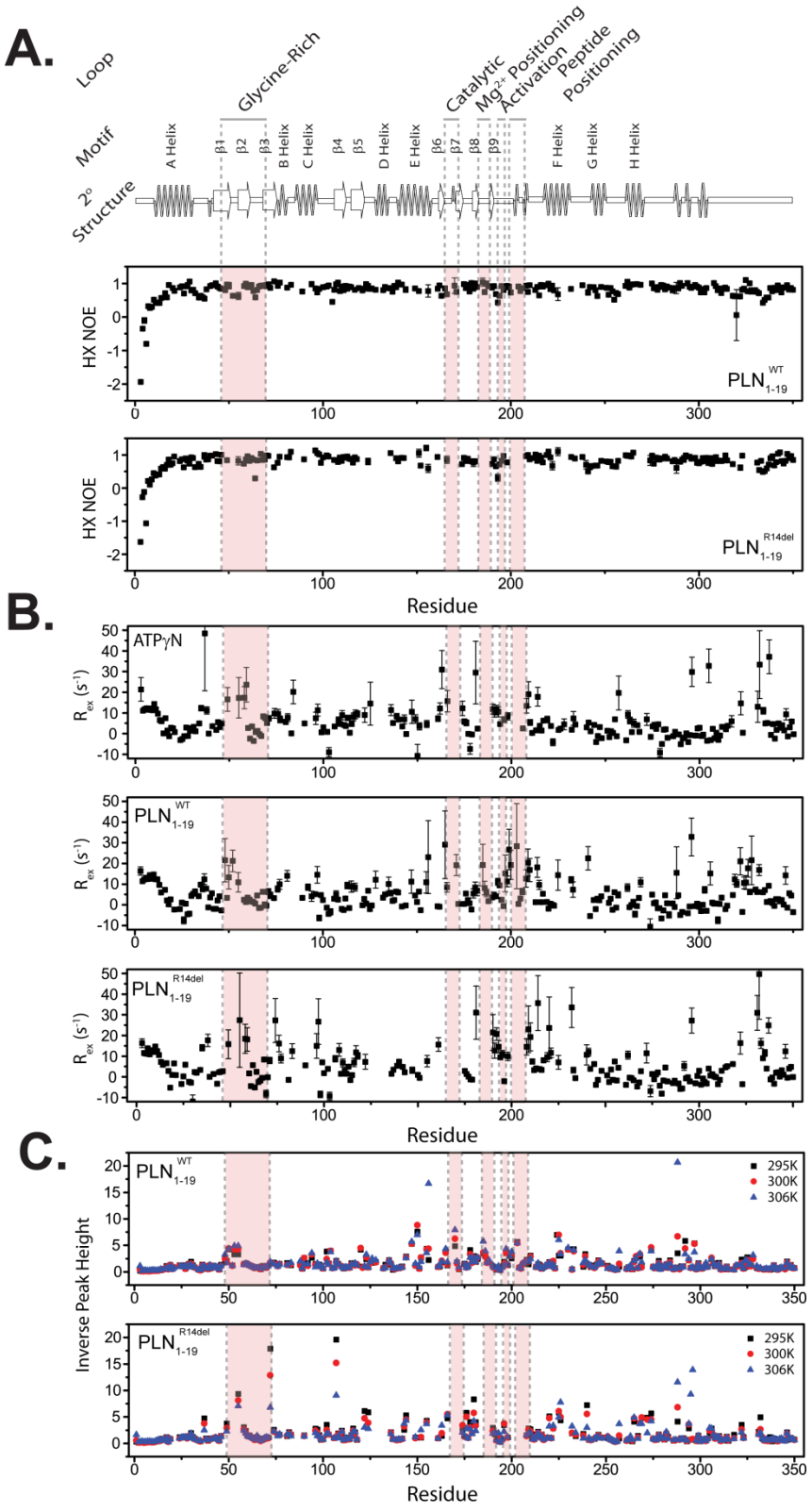
A.
Loop
Motif
2° Structure
Glycine-Rich
Catalytic
Mg2+ Positioning
Activation
Peptide
Positioning
A Helix
β1
β2
β3
B Helix
C Helix
β4
β5
D Helix
E Helix
β6
β7
β8
β9
F Helix
G Helix
H Helix
HX NOE
PLN1-19WT
PLN1-19R14del
Residue
B.
ATPγN
Rex (s-1)
PLN1-19WT
PLN1-19R14del
Residue
C.
PLN1-19WT
PLN1-19R14del
295K
300K
306K
Inverse Peak Height
Residue

Figure S10

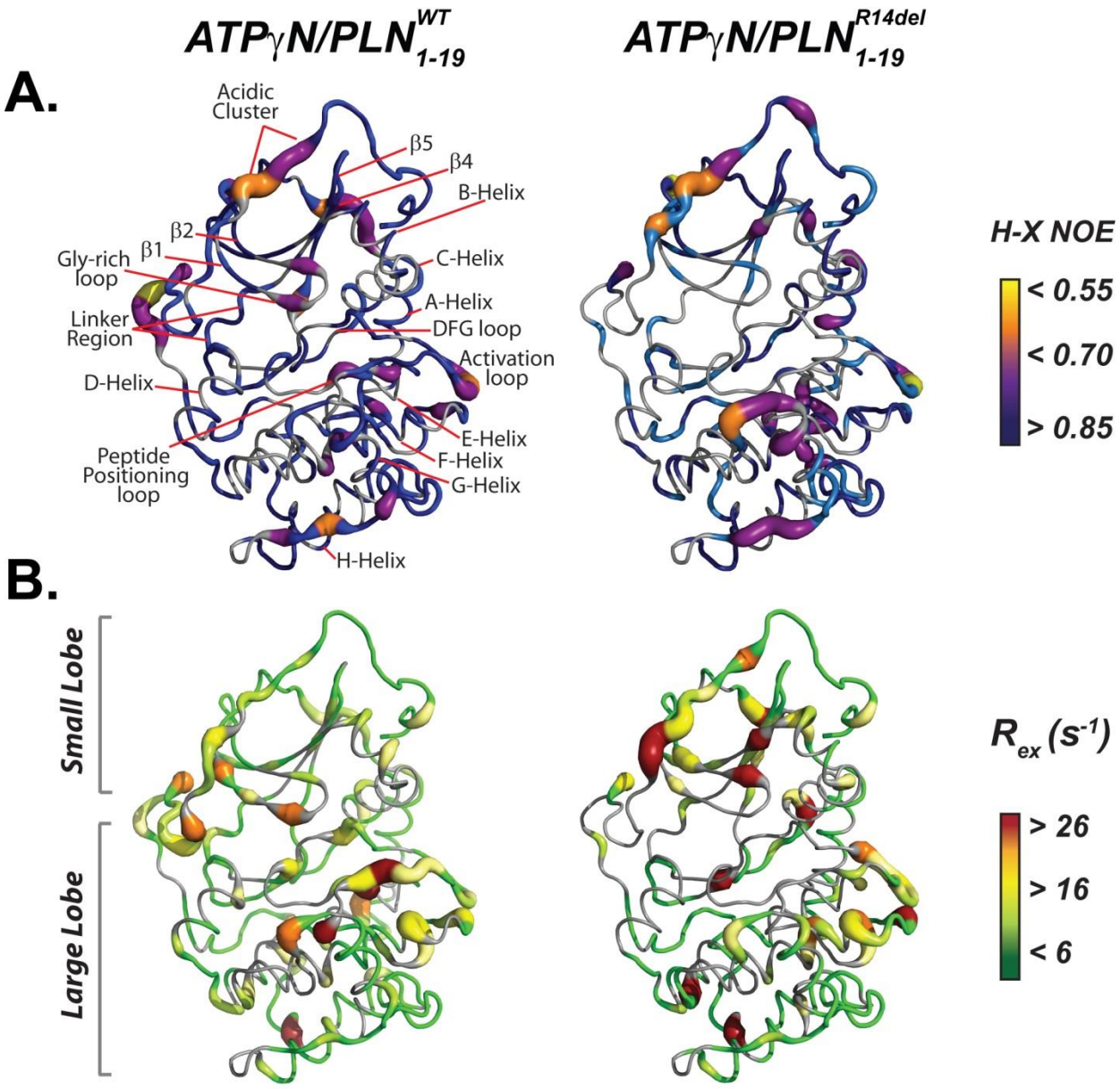
ATPγN/PLN WT 1-19
ATPγN/PLN R14del 1-19
A.
Acidic Cluster
β5
β4
B-Helix
β2
β1
Gly-rich loop
C-Helix
Linker Region
A-Helix
DFG loop
Activation loop
D-Helix
E-Helix
F-Helix
G-Helix
Peptide Positioning loop
H-Helix
H-X NOE
< 0.55
< 0.70
> 0.85
B.
Small Lobe
Large Lobe
R_ex (s^-1)
> 26
> 16
< 6

Figure S11

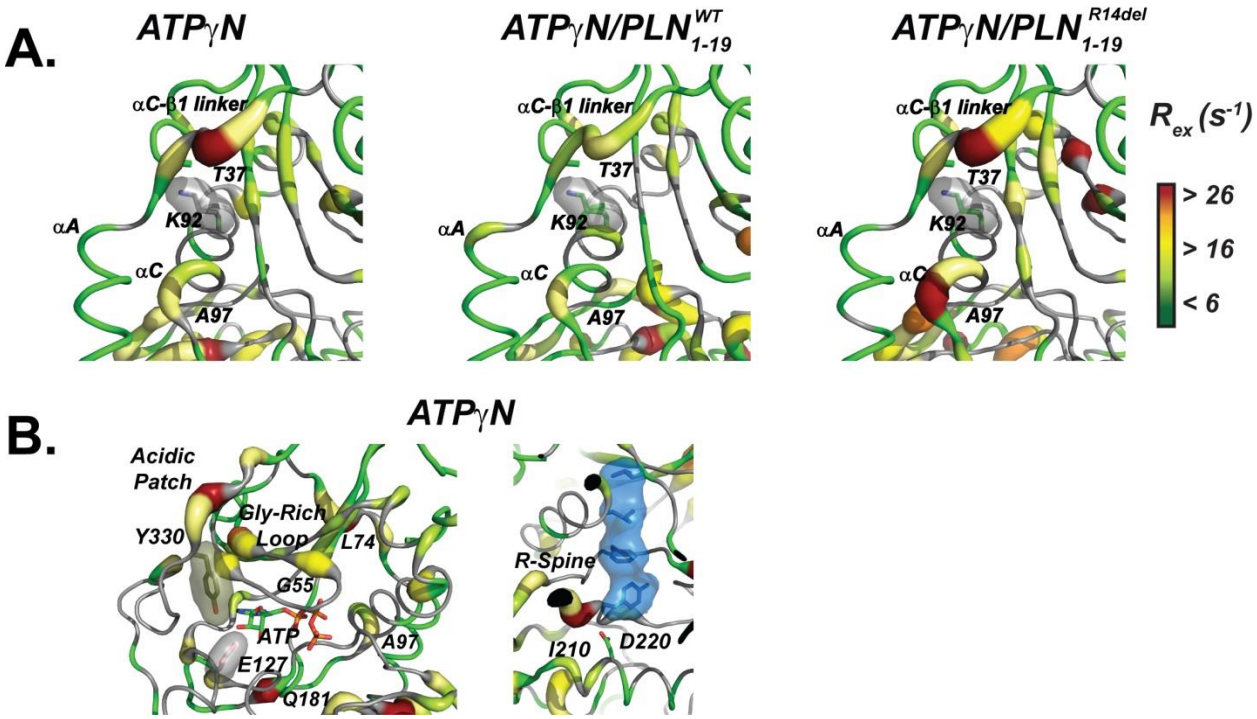
A.
ATPγN
ATPγN/PLN 1-19 WT
ATPγN/PLN 1-19 R14del
αC-β1 linker
T37
αA
K92
αC
A97
Rex (s-1)
> 26
> 16
< 6
B.
ATPγN
Acidic Patch
Gly-Rich Loop
Y330
L74
G55
ATP
A97
E127
Q181
R-Spine
I210
D220

Figure S12

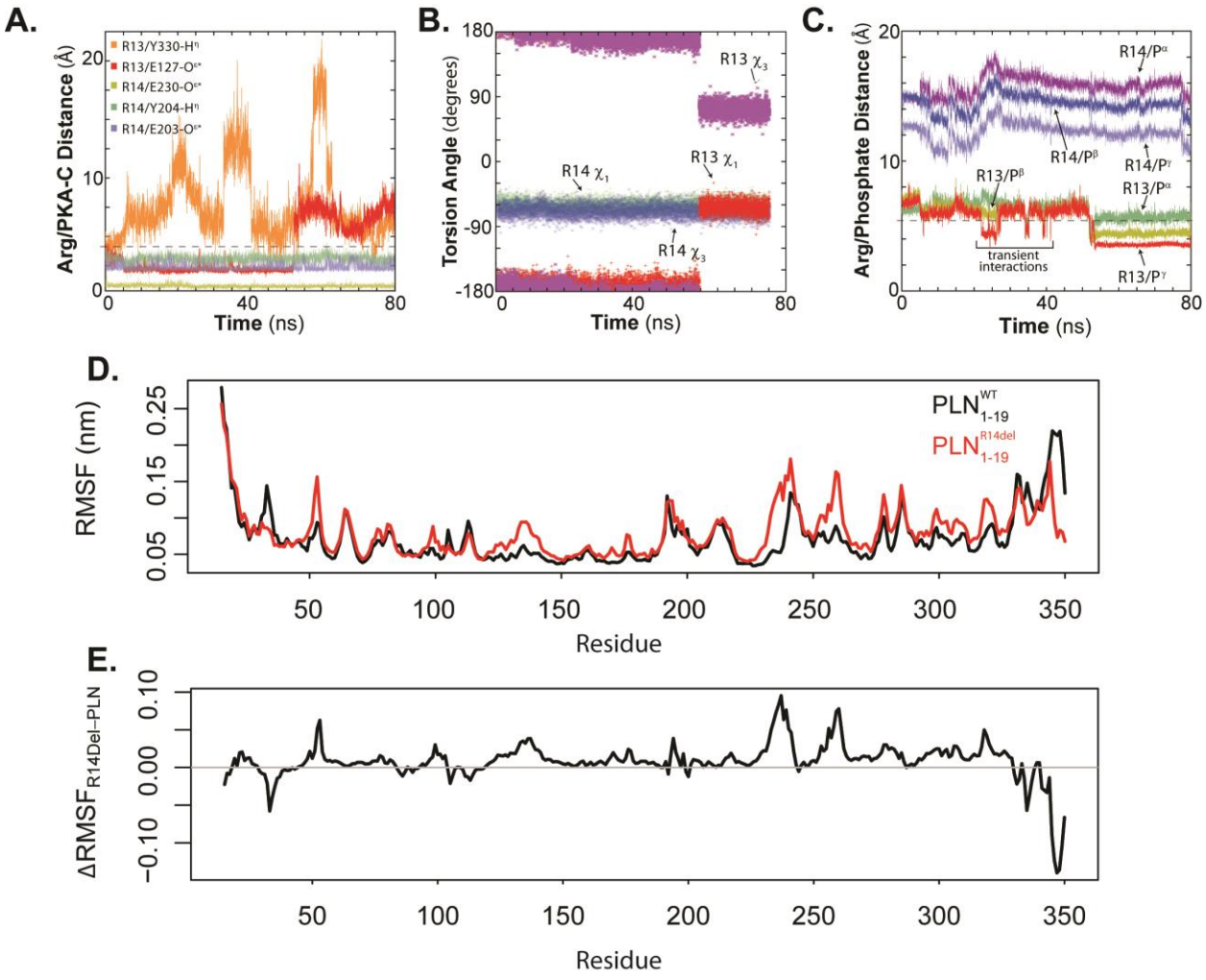
A.
Arg/PKA-C Distance (Å)
R13/Y330-Hη
R13/E127-Oε*
R14/E230-Oε*
R14/Y204-Hη
R14/E203-Oε*
Time (ns)
B.
Torsion Angle (degrees)
R13 χ3
R13 χ1
R14 χ1
R14 χ3
Time (ns)
C.
Arg/Phosphate Distance (Å)
R14/Pα
R14/Pβ
R14/Pγ
R13/Pβ
R13/Pα
transient interactions
R13/Pγ
Time (ns)
D.
RMSF (nm)
PLN1-19WT
PLN1-19R14del
Residue
E.
ΔRMSFR14Del–PLN
Residue

Table S1: Thermodynamic and kinetics parameters for PLN^{WT}_{1-19} and $\mathrm{PLN}^{R14del}_{1-19}$. Values for K_M and k_{cat} were obtained from a non-linear least squares analysis of the concentration-dependent initial phosphorylation rates using a standard coupled enzyme activity assay. Binding parameters (K_d) are derived from ITC measurements of PLN^{WT}_{1-19} or $\mathrm{PLN}^{R14del}_{1-19}$ binding to PKA-C in the presence of 2mM ATPγN. Measurements in the absence of ATPγN were only quantified for PLN^{WT}_{1-19}.

	PLN^{WT}_{1-19}	$\mathrm{PLN}^{R14del}_{1-19}$
K_d^{apo} **(μM)**	173 ± 32	-
K_d^{binary} **(μM)**	28.4 ± 2	243 ± 132
k_{cat} **(s^{-1})**	23.4 ± 1	3.8 ± 2
k_{cat}/K_M **(M^{-1} s^{-1})**	0.26 x 10^6	8.9 x 10^2

Table S2: ^{15}N relaxation and τ_c values for PLN_{1-19}^{WT} and PLN_{1-19}^{R14del}. Average HX-NOE values for both PKA-C/PLN_{1-19}^{WT} and PKA-C/PLN_{1-19}^{R14del} and the average R_{ex} value measured by Trosy Hahn-Echo. Note that even many residues in PKA-C/PLN_{1-19}^{R14del} experience R_{ex} values that escape quantitation. The rotational correlation time (τ_c) was calculated assuming isotropic rotation by dynamic light scattering.

	PLN_{1-19}^{WT}	PLN_{1-19}^{R14del}
HX-NOE	0.80 ± 0.28	0.79 ± 0.29
Trim HX-NOE	0.84 ± 0.09	0.83 ± 0.10
$\langle R_{ex} \rangle$ (s^{-1})	4.5 ± 7.1	5.0 ± 9.2
τ_c (ns)	25 ± 0.2	27 ± 0.1

Table S3: Thermodynamics of Substrate binding. The enthalpy, entropy and free energy of substrate binding to PKA-C from ITC.

	Apo/ $PLN_{1–19}^{WT}$	ATPγN $PLN_{1–19}^{WT}$	ATPγN/ $PLN_{1–19}^{R14del}$
ΔG (kcal/mol)	-5.2 ± 0.1	-6.2 ± 0.1	-5.0 ± 0.3
ΔH (kcal/mol)	-1.8 ± 0.3	-6.6 ± 0.2	-0.7 ± 0.2
TΔS (kcal/mol)	3.4 ± 0.3	-0.4 ± 0.1	4.2 ± 0.5

Table S4: List of residues that defined linear trajectories for the 5 states analyzed with CONCISE using the thresholds reported in the Methods section.

8	10	11	12	16	17	19	20	21	24
25	26	27	28	30	31	34	35	37	38
40	41	43	49	55	61	62	71	72	74
76	83	96	97	98	100	103	106	107	108
109	110	111	112	117	118	124	142	144	147
148	152	161	163	166	175	176	177	178	179
190	191	192	193	194	196	208	209	210	213
214	215	216	217	219	220	225	226	241	242
244	245	248	251	252	253	255	256	274	289
299	306	314	315	322	323	331	332	334	336
337	338	348	349	350					

Table S5: Hydrodynamic Radii from each of the individual DLS runs:

PKA/ATPγN

Z-average (nm)					
3.082	3.053	3.048	3.063	3.065	3.059

PKA/ATPγN/ $\mathrm{PLN}_{1-19}^{R14del}$

Z-average (nm)					
3.112	3.114	3.109	3.113	3.112	3.109

PKA/ATPγN/ PLN_{1-19}^{WT}

Z-average (nm)					
3.047	3.049	3.048	3.024	3.045	3.043

Table S6: Backbone HX-NOE values for PKA/ATPγN/ $\mathrm{PLN}_{1-19}^{R14del}$.

Residue	HX NOE	Residue	HX NOE	Residue	HX NOE	Residue	HX NOE
3	-1.63±0.03	67	1.03±0.01	180	0.77±0.12	288	0.60±0.15
4	-0.28±0.03	68	0.85±0.03	181	0.81±0.06	289	0.80±0.02
5	-0.12±0.06	69	0.86±0.03	190	0.73±0.05	290	0.79±0.02
6	-1.07±0.02	70	0.98±0.03	191	0.86±0.06	291	0.86±0.03
7	0.21±0.03	71	0.97±0.03	192	0.65±0.02	292	0.88±0.10
8	0.10±0.06	74	0.63±0.06	193	0.31±0.10	293	0.98±0.02
9	0.26±0.03	76	0.76±0.04	194	0.71±0.01	295	0.95±0.02
10	0.45±0.02	77	0.95±0.05	195	0.82±0.02	296	0.88±0.02
11	0.38±0,02	81	0.93±0.03	196	0.97±0.05	298	0.91±0.02
12	0.41±0.02	82	0.92±0.04	198	0.77±0.04	299	0.76±0.04
13	0.41±0.02	83	1.10±0.07	208	0.96±0.04	300	0.75±0.01
14	0.58±0.02	90	0.86±0.03	209	0.99±0.06	301	0.79±0.02
15	0.63±0.03	96	1.13±0.06	210	0.87±0.03	302	0.90±0.02
16	0.59±0.03	97	1.06±0.05	212	0.90±0.02	303	0.81±0.01
17	0.69±0.03	98	1.02±0.04	213	1.01±0.04	304	0.91±0.02
18	0.86±0.02	99	0.76±0.02	214	0.82±0.05	305	0.76±0.07
19	0.70±0.03	100	0.92±0.02	215	0.98±0.03	306	0.89±0.09
20	0.75±0.01	102	0.98±0.04	216	0.92±0.04	307	0.73±0.03
21	0.95±0.02	103	0.95±0.06	217	0.77±0.03	308	0.89±0.02
24	0.81±0.04	106	0.85±0.03	219	1.00±0.02	309	0.93±0.03
25	0.87±0.03	108	0.79±0.04	220	1.07±0.11	310	0.81±0,04
26	0.62±0.05	109	0.92±0.02	221	0.93±0.03	311	0.83±0.02
27	0.89±0.03	110	0.82±0.05	222	0.67±0.13	312	0.81±0.02
28	0.83±0.04	111	0.94±0.02	225	1.10±0.12	314	0.98±0.03
29	0.73±0,04	112	0.92±0.03	232	0.94±0.05	315	0.83±0.02
30	0.92±0.06	113	0.95±0.03	234	0.89±0.04	318	0.72±0.02
31	0.90±0.04	114	0.88±0.02	238	0.93±0.06	322	0.62±0.08
32	0.63±0.02	115	0.87±0.04	240	0.70±0.13	323	0.97±0.03
24	0.81±0,04	116	0.77±0.06	241	0.50±0.04	331	0.77±0.06
25	0.87±0.03	117	0.93±0.05	242	0.63±0.02	332	0.54±0.07
26	0.62±0.05	118	0.87±0.02	243	0.67±0.04	333	0.82±0.03
27	0.89±0.03	108	0.79±0.04	245	0.68±0.03	334	0.49±0.04
28	0.83±0.04	109	0.92±0.03	246	0.68±0.04	335	0.51±0.04
29	0.73±0.04	110	0.82±0.05	248	0.82±0.03	336	0.59±0.02
30	0.92±0.06	111	0.94±0.02	251	0.80±0.04	337	0.71±0.03
31	0.90±0.04	112	0.92±0.03	252	0.78±0.02	338	0.90±0.02
32	0.63±0.02	113	0.95±0.03	253	0.80±0.02	339	0.96±0.03
34	0.73±0.02	114	0.88±0.02	254	0.66±0.03	340	0.68±0.02
35	0.64±0.02	115	0.87±0.04	255	0.66±0.01	341	0.78±0.02

37	0.97±0.10	116	0.77±0.06	256	0.65±0.02	342	1.04±0.02
38	0.86±0.03	117	0.93±0.05	257	0.82±0.04	343	1.07±0.02
39	0.86±0.02	118	0.87±0.02	261	0.99±0.02	344	0.82±0.03
40	0.98±0.07	124	0.80±0.10	262	0.97±0.03	345	0.74±0.02
41	0.97±0.03	136	1.06±0.06	263	0.98±0.02	346	0.82±0.05
43	1.03±0.03	139	0.90±0.02	264	0.95±0.02	347	1.03±0.03
44	0.81±0.02	140	0.81±0.02	265	1.07±0.05	348	0.90±0.03
45	0.80±0.02	142	0.91±0.03	274	0.83±0.15	349	0.96±0.03
46	1.00±0.03	143	0.90±0.07	275	0.98±0.03	350	0.84±0.02
49	0.84±0.05	151	1.05±0.12	276	0.74±0.03		
55	0.82±0.12	152	0.68±0.04	277	0.92±0.02		
58	0.73±0.05	156	0.59±0.13	278	0.90±0.04		
59	0.86±0.05	161	0.94±0.03	279	0.86±0.03		
60	0.96±0.03	166	0.85±0.11	280	0.89±0.03		
61	0.82±0.04	174	0.72±0.06	281	0.89±0.02		
62	0.90±0.03	175	0.91±0.04	282	0.94±0.03		
63	0.86±0.03	176	0.84±0.10	283	0.89±0.04		
64	0.29±0.06	177	0.88±0.03	286	0.81±0.02		
65	0.84±0.04	179	0.81±0.08	287	0.85±0.02		

Table S7: Backbone HX-NOE values for PKA/ATPγN/ $\mathrm{PLN}^{WT}_{1–19}$.

Residue	HX NOE	Residue	HX NOE	Residue	HX NOE	Residue	HX NOE
3	-1.94±0.05	77	1.02±0.05	186	0.74±0.08	278	0.81±0.06
4	-0.35±0.03	81	0.87±0.03	187	1.00±0.04	279	0.89±0.02
5	-0.11±0.08	83	0.96±0.05	188	0.92±0.07	280	0.95±0.03
6	-0.80±0.02	89	0.76±0.05	190	0.88±0.04	281	0.94±0.03
7	0.32±0.02	94	0.98±0.08	191	0.92±0.03	282	0.82±0.04
8	0.27±0.03	96	0.85±0.03	192	0.68±0.03	283	0.91±0.02
9	0.30±0.03	97	0.73±0.04	193	0.43±0.06	284	0.88±0.06
10	0.51±0.02	98	0.83±0.05	194	0.63±0.03	286	0.79±0.02
11	0.43±0.03	100	0.88±0.02	195	0.92±0.02	287	0.86±0.03
12	0.42±0.02	102	0.90±0.05	196	0.80±0.08	288	0.86±0.17
13	0.41±0.03	103	0.94±0.05	197	0.89±0.08	289	0.85±0.02
14	0.56±0.03	105	0.45±0.04	198	0.93±0.05	290	1.01±0.03
16	0.71±0.02	106	0.81±0.03	199	0.91±0.06	291	0.93±0.04
17	0.59±0.03	107	0.97±0.05	200	0.73±0.07	294	1.00±0.08
18	0.95±0.02	108	1.02±0.04	204	0.91±0.03	295	0.90±0.03
20	0.86±0.03	109	0.77±0.04	205	0.77±0.02	296	0.87±0.03
21	0.77±0.04	110	0.91±0.04	206	0.86±0.04	298	0.95±0.02
24	0.88±0.04	111	0.80±0.02	208	0.93±0.06	299	0.91±0.05
25	0.92±0.04	112	0.93±0.03	209	0.74±0.06	300	0.88±0.03
26	0.70±0.03	113	0.84±0.03	210	0.94±0.06	301	0.73±0.03
27	0.91±0.02	114	0.91±0.02	213	0.80±0.04	302	0.83±0.03
28	0.95±0.04	115	0.88±0.05	214	0.90±0.05	303	0.73±0.05
29	1.06±0.04	117	0.81±0.04	215	0.64±0.03	304	0.86±0.03
30	0.79±0.05	119	0.86±0.03	216	0.95±0.02	308	1.01±0.03
31	0.81±0.03	121	0.79±0.03	217	0.91±0.03	309	0.92±0.03
32	0.71±0.03	122	0.84±0.04	214	0.82±0.05	310	0.80±0.04
34	0.58±0.03	123	0.98±0.07	215	0.98±0.03	311	0.85±0.02
35	0.63±0.02	124	0.93±0.03	216	0.92±0.04	312	0.71±0.03
36	0.58±0.06	125	0.84±0.06	217	0.77±0.03	314	0.87±0.03
37	0.55±0.05	126	0.85±0.05	219	0.95±0.04	315	0.83±0.02
38	0.82±0.03	128	0.81±0.05	220	0.99±0.05	318	0.63±0.03
40	0.92±0.04	132	0.80±0.04	221	0.83±0.04	319	0.62±0.05
41	0.95±0.02	133	0.89±0.03	222	0.93±0.08	320	0.05±0.76
42	0.94±0.03	135	0.85±0.06	223	0.79±0.02	322	0.61±0.07
43	1.00±0.03	136	0.86±0.06	225	0.68±0.19	323	0.81±0.02
44	0.90±0.04	137	0.75±0.03	232	0.84±0.02	324	0.84±0.04
45	0.86±0.02	138	0.93±0.02	238	0.94±0.03	325	1.10±0.07
46	0.84±0.04	139	0.89±0.03	241	0.73±0.08	326	0.76±0.03
48	0.80±0.07	140	1.02±0.03	242	0.89±0.04	327	1.01±0.05

49	0.97±0.05	142	0.97±0.03	244	0.89±0.02	328	0.77±0.09
50	0.93±0.10	144	0.82±0.08	245	0.80±0.05	330	0.80±0.04
52	0.63±0.05	149	0.85±0.04	246	0.62±0.07	331	0.75±0.02
55	0.62±0.11	151	0.77±0.03	248	0.90±0.04	332	0.71±0.03
58	0.92±0.05	156	0.77±0.19	251	0.87±0.03	334	0.42±0.06
59	0.99±0.05	161	0.84±0.03	252	0.66±0.03	335	0.51±0.04
60	0.89±0.06	162	0.94±0.03	253	0.86±0.03	336	0.58±0.04
61	0.92±0.04	163	0.63±0.05	254	0.77±0.03	337	0.58±0.03
62	0.95±0.03	165	0.85±0.07	255	0.51±0.04	338	0.86±0.03
63	0.77±0.04	166	0.67±0.06	256	0.71±0.03	339	0.76±0.04
64	0.59±0.04	170	0.93±0.23	257	0.68±0.07	340	0.87±0.02
65	0.80±0.02	171	0.74±0.06	261	0.93±0.02	341	0.80±0.02
66	0.91±0.02	175	0.98±0.06	262	1.05±0.03	342	0.94±0.03
67	0.93±0.02	176	0.86±0.03	263	0.87±0.03	343	0.80±0.03
68	0.94±0.03	177	0.96±0.03	264	0.96±0.02	344	0.73±0.04
69	0.92±0.03	178	0.77±0.08	265	0.97±0.05	345	0.88±0.02
70	0.95±0.03	179	1.01±0.06	267	0.98±0.04	346	0.88±0.06
71	0.97±0.04	180	0.85±0.07	269	0.96±0.02	347	0.94±0.05
72	0.87±0.05	181	1.00±0.06	275	1.00±0.03	348	0.81±0.05
74	1.06±0.05	182	0.89±0.07	276	0.85±0.03	349	0.86±0.03
76	0.93±0.03	185	1.03±0.12	277	0.89±0.03	350	0.81±0.03

Table S8: Backbone R_{ex} values for PKA/ATPγN from the Trosy Hahn-Echo Experiment.

Residue	R_{ex} (s^{-1})	Residue	R_{ex} (s^{-1})	Residue	R_{ex} (s^{-1})	Residue	R_{ex} (s^{-1})
16	7.49±0.91	97	11.36±2.89	206	2.51±0.73	282	2.17±0.79
17	1.52±0.22	99	0.65±0.10	208	13.45±3.47	283	-1.96±0.36
18	-1.19±0.14	100	3.10±0.17	209	19.05±6.11	286	-1.22±0.15
19	2.90±0.50	102	0.91±2.19	210	5.40±1.39	287	0.82±0.12
20	2.59±0.28	103	-8.98±2.19	211	0.36±0.06	289	-0.40±0.06
21	0.79±0.11	106	3.44±0.57	213	1.62±0.35	290	-5.10±0.83
24	-3.12±0.50	108	6.53±1.53	214	17.85±4.58	291	-2.27±0.40
25	-2.63±0.41	109	4.73±0.78	215	3.79±0.64	292	-1.84±0.59
26	-1.23±0.23	110	8.94±2.20	216	1.53±0.34	293	0.11±0.01
27	2.93±0.57	111	4.22±0.59	217	6.30±0,94	294	-4.04±1.10
28	-1.12±0.20	112	3.65±0.64	219	6.81±1.58	295	-0.75±0.10
29	1.34±0.28	113	7.59±1.32	221	3.69±0.64	296	29.88±7.02
30	2.59±0.65	114	0.40±0.07	222	-4.20±1.68	298	-0.88±0.10
31	3.30±0.65	115	4.84±1.33	225	1.76±0.81	299	2.52±0.67
32	1.14±0.16	116	8.05±1.89	226	2.39±1.09	300	2.89±0.27
34	4.92±0.56	117	9.29±2.09	228	4.53±2.61	301	-1.13±0.15
35	12.27±1.30	118	9.52±1.49	232	1.91±0.39	302	-0.53±0.06
37	48.49±27.71	122	8.98±3.47	233	7.32±3.35	304	-3.47±0.49
38	11.23±1.80	125	14.53±10.43	234	4.45±1.17	305	32.79±8.12
39	0.05±0.01	136	11.39±2.65	240	3.02±0.52	306	-3.10±0.75
41	3.56±0.49	137	5.17±0.69	241	5.34±0.89	307	2.30±0.43
43	1.82±0.28	139	8.46±1.28	242	1.20±0.13	308	-2.27±0.40
44	5.58±0.82	140	6.87±1.06	244	4.20±0.56	309	0.42±0.07
45	3.15±0.39	142	3.46±0.59	245	-4.05±0.67	310	-3.06±0.57
46	4.92±1.08	143	6.90±2.12	246	-1.15±0.22	311	-0.95±0.12
49	16.55±5.77	144	-0.21±0.10	247	3.14±0.56	312	3.30±0.40
55	17.29±9.77	147	10.57±5.63	248	-2.14±0.33	314	2.12±0.36
58	17.37±5.30	149	7.08±2.00	251	1.35±0.26	315	3.79±0.48
59	23.68±8.37	150	-10.72±5.47	252	-1.62±0.25	317	5.98±2.69
60	2.74±0.58	151	3.56±1.73	253	1.15±0.16	322	14.66±5.53
61	-2.38±0.48	155	4.66±1.71	254	0.29±0.03	323	0.42±0.07
62	3.50±0.67	161	7.22±1.36	255	6.95±0.65	331	12.99±7.52
63	-3.50±0.57	162	12.16±2.68	256	-1.23±0.13	332	33.43±16.42
64	0.80±0.11	163	31.01±9.19	257	19.64±8.24	334	11.09±1.63
65	1.28±0.25	166	15.67±5.14	261	-3.22±0.40	335	4.93±0.62
66	-0.29±0.05	174	12.22±3.54	262	9.28±1.78	336	5.17±0.59
67	-1.13±0.12	175	5.85±1.34	263	6.36±1.58	337	37.16±8.18
68	8.33±1.18	176	5.17±1.41	264	0.72±0.10	338	-0.59±0.08
69	7.69±1.42	177	-0.06±0.01	265	5.08±1.92	339	4.59±0.64

70	5.16±0.96	178	-7.37±2.55	267	4.07±0.52	340	-2.38±0.30
71	7.39±1.35	179	-0.44±0.11	268	0.91±0.37	341	1.78±0.20
74	9.80±2.31	181	29.55±15.18	272	6.90±2.89	342	4.99±0.81
76	9.54±2.20	182	2.42±1.03	274	-1.51±0.47	343	2.81±0.45
77	6.86±1.60	190	11.87±2.34	275	3.51±0.59	344	4.15±0.62
80	5.69±1.26	191	10.23±2.26	276	4.33±0.59	345	1.56±0.19
81	7.73±1.89	192	11.39±2.37	277	2.29±0.32	346	9.37±2.73
83	0.17±0.03	193	10.55±2.44	278	4.53±1.08	347	-1.37±0.25
84	20.16±5.73	194	4.64±0.39	279	-9.19±2.03	348	3.11±0.54
90	4.96±1.02	196	6.73±1.42	280	-5.01±0.77	349	5.93±0.94
96	7.43±3.00	198	8.37±1.72	281	1.91±0.30	350	-0.30±0.04

Table S9: Backbone R_{ex} values for PKA/ATPγN/ PLN_{1-19}^{R14del} from the Trosy Hahn-Echo Experiment.

Residue	R_{ex} (s^{-1})	Residue	R_{ex} (s^{-1})	Residue	R_{ex} (s^{-1})	Residue	R_{ex} (s^{-1})
16	6.58±0.78	106	8.81±1.52	209	23.05±11.27	289	-3.26±0.47
17	2.90±0.40	108	13.04±3.05	210	19.31±6.73	290	-5.88±0.90
18	-5.15±0.58	109	1.49±0.25	211	7.43±1.27	291	-5.65±0.93
19	0.95±0.15	110	6.78±1.93	212	3.26±0.50	292	5.26±2.09
20	6.51±0.54	111	3.11±0.41	213	4.14±0.75	293	-0.70±0.08
21	0.89±0.12	112	1.45±0.27	214	35.69±13.33	294	-0.17±0.04
24	-3.37±0.53	113	4.93±0.68	215	3.79±0.78	295	-2.18±0.28
25	0.28±0.04	114	-1.56±0.25	216	3.41±0.79	296	27.19±6.08
26	5.93±0.90	115	0.91±0.25	217	8.02±1.25	298	-3.10±0.55
28	-2.33±0.37	116	6.97±2.08	219	9.58±2.29	299	0.41±0.09
29	-2.83±0.54	117	11.88±3.20	220	23.67±14.90	300	2.92±0.27
30	-11.86±3.07	118	10.15±1.56	221	11.62±2.34	301	-3.77±0.45
31	2.34±0.44	108	13.04±3.05	225	7.04±3.38	302	-0.77±0.09
32	1.96±0.23	109	1.49±0.25	232	33.57±9.67	303	-2.52±0.28
34	3.39±0.35	110	6.78±1.93	233	3.28±1.37	304	-3.20±0.43
35	14.08±1.48	111	3.11±0.41	234	-0.59±0.13	305	3.96±1.15
38	17.65±2.97	112	1.45±0.27	240	10.65±4.89	306	0.61±0.15
39	0.02±0.00	113	4.93±0.68	241	11.98±1.88	307	1.28±0.22
41	1.37±0.18	114	-1.56±0.25	242	3.94±0.44	308	0.25±0,03
43	-3.37±0.59	115	0.91±0.25	244	6.18±0.89	309	-0.17±0.03
44	2.18±0.33	116	6.97±2.08	245	-3.82±0.63	310	-3.55±0.64
45	2.51±0.28	117	11.88±3.20	246	-1.47±0.29	311	-1.48±0.17
49	15.78±6.98	118	10.15±1.56	248	2.99±0.55	312	2.97±0.33
55	27.41±22.79	122	7.28±3.64	251	0.77±0.15	314	4.62±0.77
58	18.43±7.04	136	1.45±0.38	252	-2.44±0.36	315	5.13±0.61
59	18.07±5.66	137	3.53±0.42	253	3.55±0.50	318	6.16±0.77
60	1.68±0.35	139	5.36±0.76	254	-1.47±0.16	322	16.37±5.33
61	-4.50±0.94	140	7.40±1.05	255	7.44±0.63	323	-3.48±0.56
62	5.70±1.16	142	4.84±0.83	256	-1.76±0.17	331	30.93±8.46
63	-5.06±0.8	143	2.24±0.83	257	4.44±1.14	332	49.66±21.77
64	2.46±0.32	147	3.24±1.54	261	-3.81±0.44	333	16.19±2.42
65	-2.48±0.44	150	0.96±0.57	262	10.53±1.96	334	9.05±1.10
66	-1.75±0.29	140	7.40±1.05	263	-0.40±0.07	335	11.58±1.58
67	-0.45±0.05	151	-0.48±0.24	264	-0.59±0.08	336	3.97±0.41
68	8.43±1.09	155	7.63±2.80	265	-1.68±0.65	337	24.90±3.72
69	-8.25±1.80	161	15.64±3.30	267	-4.65±0.72	338	-1.19±0.17
70	-0.15±0.03	175	2.87±0.60	268	-2.73±±0.94	339	-0.34±0.05
71	7.91±1.48	176	1.38±0.53	269	2.69±1.02	340	-3.30±0.42

74	27.31±10.62	177	0.15±0.03	272	11.45±4.73	341	2.06±0.21
76	16.15±3.97	178	-1.21±0.39	274	-6.88±2.71	342	2.21±0.34
77	8.89±2.17	179	-1.36±0.34	275	1.36±0.21	343	0.15±0.02
81	-1.44±0.33	181	31.04±12.86	276	-1.14±0.15	344	3.17±0.46
83	12.45±3.55	190	21.47±8.72	277	1.15±0.16	345	1.12±0.14
90	5.56±1.17	191	12.65±3.67	278	2.13±0.49	346	12.40±3.36
96	15.01±5.98	192	20.70±3.08	279	-4.22±0.91	347	-0.36±0.06
97	26.73±11.01	193	14.61±2.94	280	-8.09±1.21	348	4.01±0.69
98	-8.46±1.55	194	9.42±0.88	281	-1.74±0.25	349	4.85±0.74
99	6.98±1.05	195	11.06±1.70	282	4.53±1.01	350	-0.12±0.02
100	1.78±0.25	196	-2.04±0.72	283	-2.20±0.41		
102	3.85±0.72	198	9.92±2.06	286	-3.02±0.37		
103	-9.30±1.91	208	14.52±3.90	287	-1.83±0.26		

Table S10: Backbone R_{ex} values for PKA/ATPγN/ PLN_{1-19}^{WT} from the Trosy Hahn-Echo Experiment.

Residue	R_{ex} (s^{-1})	Residue	R_{ex} (s^{-1})	Residue	R_{ex} (s^{-1})	Residue	R_{ex} (s^{-1})
16	7.28±0.98	103	-4.34±1.52	196	-0.59±0.15	288	15.48±12.53
17	2.13±0.34	104	-3.36±1.52	197	15.19±8.92	289	4.61±0.68
18	0.25±0.03	106	2.99±0.45	198	11.31±2.64	290	-4.89±0.86
19	2.69±0.58	107	5.06±1.75	199	26.73±9.80	291	-3.47±0.64
21	-2.28±0.40	108	2.51±0.59	200	19.31±7.06	294	-4.06±1.19
24	-2.06±0.41	110	-1.94±0.47	203	28.40±20.61	295	-0.77±0.12
25	1.09±0.21	111	-2.45±0.36	204	0.40±0.07	296	32.81±9.20
26	-7.49±1.66	112	3.11±0.56	205	3.06±0.42	298	-0.58±0.08
27	0.60±0.08	113	9.34±1.54	206	6.43±1.51	299	0.58±0.16
28	-4.53±0.86	114	-1.52±0.28	208	12.69±4.24	300	-0.89±0.14
29	-4.26±0.98	115	8.82±2.69	209	20.47±6.49	301	-3.03±0.42
30	4.37±1.21	117	8.54±1.92	210	16.85±5.59	302	0.02±0.00
31	5.32±0.96	121	-0.20±0.03	213	1.31±0.24	303	7.23±1.58
32	6.53±0.97	122	2.86±0.53	214	18.10±4.80	304	-2.93±0.44
34	4.23±0.43	123	0.70±0.25	215	9.67±2.22	306	15.22±5.53
35	9.77±1.01	124	6.77±1.15	216	1.26±0.16	307	1.10±0.23
36	7.99±1.73	125	-2.06±0.54	217	5.36±0.91	308	0.51±0.09
37	12.41±2.56	126	-0.24±0.07	219	1.40±0.32	309	0.68±0.14
38	7.84±1.15	128	12.20±4.15	220	-1.82±0.54	310	-7.45±1.65
39	-1.26±0.16	132	3.51±0.51	221	0.55±0.11	311	0.44±0.06
40	3.59±0.69	133	5.03±0.86	222	0.04±0.01	312	3.52±0.44
41	5.57±0.76	135	10.09±3.56	223	-0.36±0.05	314	-2.11±0.32
42	-2.00±0.36	136	5.67±1.56	225	14.33±7.31	315	-0.40±0.05
43	-1.94±0.34	137	1.94±0.24	232	12.10±1.51	318	4.72±0.53
44	2.11±0.40	138	2.36±0.31	233	7.38±3.72	319	12.35±2.37
45	4.13±0.52	139	6.39±1.03	241	22.52±5.62	320	10.28±1.77
46	-2.74±0.65	140	6.02±0.99	242	-5.44±1.04	322	21.03±6.59
48	21.59±10.47	142	-0.76±0.13	244	2.33±0.31	323	-3.45±0.45
49	3.36±1.15	144	-0.25±0.11	245	-2.05±0.40	324	10.60±2.89
50	13.35±5.71	147	11.23±5.63	246	2.95±0.74	325	10.82±3.32
52	21.24±5.21	149	4.53±0.95	247	2.20±0.53	326	17.71±4.30
55	10.88±4.69	150	1.36±0.72	248	4.08±1.01	327	6.21±1.30
58	2.38±0.54	151	6.39±0.91	251	7.76±1.40	328	21.56±11.77
59	1.34±0.39	152	-2.59±0.79	252	0.93±0.12	330	7.36±1.29
60	3.46±1.00	155	10.88±5.17	253	2.96±0.49	331	6.22±0.81
61	2.54±0.65	156	23.07±17.63	254	-2.37±0.28	332	16.82±2.68
62	1.55±0.33	161	-0.71±0.14	255	6.11±0.62	334	6.08±0.66
63	1.35±0.26	162	-0.89±0.20	256	-1.34±0.16	335	7.12±0.92

64	0.66±0.10	165	29.05±16.38	257	4.85±1.44	336	1.37±0.15
65	4.52±0.75	166	8.52±2.33	262	8.30±1.84	337	9.19±1.11
66	-1.54±0.28	171	19.20±5.06	263	-1.11±0.21	338	1.81±0.28
67	-1.31±0.17	172	0.49±0.07	264	-0.03±0.00	339	0.83±0.18
68	6.29±1.13	175	0.43±0.11	265	1.49±0.40	340	-0.49±0.07
69	0.21±0.05	176	5.51±0.91	266	-4.52±1.38	341	2.76±0.33
70	-0.35±0.06	177	2.28±0.45	267	-0.56±0.09	342	2.77±0.45
71	6.43±1.49	178	0.71±0.27	268	3.33±1.23	343	1.75±0.28
72	4.61±1.56	179	-2.27±0.70	269	10.89±2.23	344	2.37±0.39
74	3.22±0.90	180	5.51±2.27	274	-10.51±3.72	345	0.14±0.02
76	7.62±1.46	181	8.36±2.59	275	4.96±0.89	346	14.24±4.23
77	9.93±2.32	182	6.78±2.38	276	0.81±0.13	347	-1.30±0.25
81	14.04±2.64	185	19.25±10.08	277	1.18±0.19	348	5.55±1.07
89	3.40±0.47	186	8.09±3.30	278	-1.60±0.46	349	4.48±0.72
92	8.51±1.52	187	5.76±1.85	279	-1.60±0.25	350	-3.51±0.56
94	4.15±2.43	188	1.82±0.73	280	-6.59±1.12		
96	5.11±1.04	190	3.56±0.74	281	-2.68±0.43		
97	14.54±4.02	191	4.98±0.82	282	4.64±1.15		
98	-6.33±1.34	192	4.08±0.56	283	0.75±0.12		
99	4.76±0.93	193	11.07±1.68	284	-4.86±1.51		
100	2.35±0.32	194	9.44±0.99	286	0.66±0.09		
102	-1.36±0.27	195	2.42±0.42	287	-0.99±0.17		

References

1. Wiseman, T., et al., *Rapid Measurement of Binding Constants and Heats of Binding Using a New Titration Calorimeter.* Analytical Biochemistry, 1989. **179**(1): p. 131-137.
2. Delaglio, F., et al., *NMRPipe: A multidimensional spectral processing system based on UNIX pipes.* Journal of Biomolecular NMR, 1995. **6**(3): p. 277-293.
3. Salzmann, M., et al., *TROSY-type triple-resonance experiments for sequential NMR assignments of large proteins.* Journal of the American Chemical Society, 1999. **121**(4): p. 844-848.
4. Salzmann, M., et al., *TROSY in triple-resonance experiments: new perspectives for sequential NMR assignment of large proteins.* Proc Natl Acad Sci U S A, 1998. **95**(23): p. 13585-90.
5. Farrow, N.A., et al., *Backbone dynamics of a free and phosphopeptide-complexed Src homology 2 domain studied by 15N NMR relaxation.* Biochemistry, 1994. **33**(19): p. 5984-6003.
6. Pervushin, K., et al., *Attenuated T2 relaxation by mutual cancellation of dipole–dipole coupling and chemical shift anisotropy indicates an avenue to NMR structures of very large biological macromolecules in solution.* Proceedings of the National Academy of Sciences, 1997. **94**(23): p. 12366-12371.
7. Wang, C., M. Rance, and A.G. Palmer, 3rd, *Mapping chemical exchange in proteins with MW > 50 kD.* J Am Chem Soc, 2003. **125**(30): p. 8968-9.
8. Fenwick, M.K. and R.E. Oswald, *NMR spectroscopy of the ligand-binding core of ionotropic glutamate receptor 2 bound to 5-substituted willardiine partial agonists.* J Mol Biol, 2008. **378**(3): p. 673-85.
9. Cembran, A., et al., *NMR mapping of protein conformational landscapes using coordinated behavior of chemical shifts upon ligand binding.* Phys Chem Chem Phys, 2014. **16**(14): p. 6508-18.
10. Selvaratnam, R., et al., *Mapping allostery through the covariance analysis of NMR chemical shifts.* Proc Natl Acad Sci U S A, 2011. **108**(15): p. 6133-8.
11. Masterson, L.R., et al., *Dynamically committed, uncommitted, and quenched states encoded in protein kinase A revealed by NMR spectroscopy.* Proc Natl Acad Sci U S A, 2011. **108**(17): p. 6969-74.
12. Brooks, B.R., et al., *CHARMM: the biomolecular simulation program.* J Comput Chem, 2009. **30**(10): p. 1545-614.
13. Phillips, J.C., et al., *Scalable molecular dynamics with NAMD.* J Comput Chem, 2005. **26**(16): p. 1781-802.
14. MacKerell, A.D., Jr., N. Banavali, and N. Foloppe, *Development and current status of the CHARMM force field for nucleic acids.* Biopolymers, 2000. **56**(4): p. 257-65.
15. Mackerell, A.D., Jr., M. Feig, and C.L. Brooks, 3rd, *Extending the treatment of backbone energetics in protein force fields: limitations of gas-phase quantum mechanics in reproducing protein conformational distributions in molecular dynamics simulations.* J Comput Chem, 2004. **25**(11): p. 1400-15.
16. Martyna, G.J., D.J. Tobias, and M.L. Klein, *Constant-Pressure Molecular-Dynamics Algorithms.* Journal of Chemical Physics, 1994. **101**(5): p. 4177-4189.

17. Darden, T., et al., *New tricks for modelers from the crystallography toolkit: the particle mesh Ewald algorithm and its use in nucleic acid simulations.* Structure with Folding & Design, 1999. **7**(3): p. R55-R60.
18. Andersen, H.C., *Rattle: A "velocity" version of the shake algorithm for molecular dynamics calculations.* Journal of Computational Physics, 1983. **52**(1): p. 24-34.
19. Tuckerman, M., B.J. Berne, and G.J. Martyna, *Reversible Multiple Time Scale Molecular-Dynamics.* Journal of Chemical Physics, 1992. **97**(3): p. 1990-2001.